 doi:10.20944/preprints202211.0092.v1

Article

Physicochemical, Morphological and Cytotoxic properties of Brazilian Jackfruit (*Artocarpus Eterophyllus*) Starch Scaffold loaded with Silver Nanoparticles

José Filipe Bacalhau Rodrigues *, Valeriano Soares Azevedo, Rebeca Peixoto Medeiros, Gislaine Bezerra de Carvalho Barreto, Maria Roberta de Oliveira Pinto, Marcus Vinicius Lia Fook and Maziar Montazerian *

Academic Unit of Materials Science and Engineering, Federal University of Campina Grande, PB, Brazil; filipe.rodrigues@certbio.ufcg.edu.br (J.F.B.R.); valeriano11@hotmail.com (V.S.A.); rebeca.peixoto@certbio.ufcg.edu.br (R.P.M.); gislainecarvalho11@hotmail.com (G.B.C.B.); roberta.oliveira@certbio.ufcg.edu.br (M.R.O.P.); marcus.liafook@certbio.ufcg.edu.br (M.V.L.F.); maziar_montaz@yahoo.com (M.M.)

* Correspondence: filipe.rodrigues@certbio.ufcg.edu.br; Tel.: +55 83 991284865 (J.F.B.R.); maziar_montaz@yahoo.com; Tel: +55 83 99401 1889 (M.M.)

Abstract: Starch is a widespread natural polymer used in healthcare applications due to its low cost and antibacterial properties. The use of starch in its many forms and its sometimes combination with metallic nanoparticles have all contributed to the advancement of biomaterials. However, few studies have been conducted on biocomposites composed of jackfruit starch and silver nanoparticles (AgNPs). As a result, this research aims to study the physicochemical, morphological, and cytotoxic features of a Brazilian jackfruit (*Artocarpus heterophyllus*) starch-based scaffold loaded with AgNPs. Gelatinization and chemical reduction were used to synthesize the scaffold and AgNPs, respectively. X-ray diffraction (XRD), differential scanning calorimetry (DSC), scanning electron microscopy coupled with energy-dispersive spectroscopy (SEM-EDS), and Fourier transform infrared spectroscopy (FTIR) were utilized to explore the properties. The findings supported the development of anisotropic, stable, monodispersed AgNPs. The presence of AgNPs in the scaffold matrix was revealed by XRD and SEM-EDS. AgNPs were found to modify the crystallinity, roughness, and thermal stability of the scaffold while leaving its chemical and physical characteristics unchanged. Finally, the scaffolds did not show adverse effects on the L929 cells.

Keywords: Jackfruit; Silver; Nanoparticles; Scaffold; Biomaterials

1. Introduction

Scaffolds are three-dimensional porous structures that facilitate tissue growth/remodeling by supporting human cell adhesion, proliferation, differentiation, and orientation in a stable environment. They are commonly employed in biomedical tissue engineering and are made of biocompatible and biodegradable materials that allow for the incorporation and transport of medicines and biological components [1–4].

Starch is a low-cost, biodegradable, biocompatible, and natural polymer widely used in fabricating scaffolds [5–8]. Amylose (glucose units joined by α-1,4-glycosidic bonds) and amylopectin (glucose units linked by glycosidic bonds at α-1,4 and α-1,6 carbons) chains make up starch's molecular structure [9]. Starch, like other polysaccharides and proteins, is a thermoplastic polymer composed of linear chains linked by weak bonds and capable of being processed into membranes [10], gels [11], nanofibers [12], microparticles [13], nanoparticles [14], and scaffolds [6]. It can also encapsulate pharmaceuticals and metallic nanoparticles that bond to the long polymeric chains and hydroxyl groups of molecular structure [15,16].

 doi:10.20944/preprints202211.0092.v1

Silver nanoparticles (AgNPs) stand out among metallic nanoparticles due to their distinctive physical, chemical, and biological features, particularly antibacterial and antifungal activities [17], simple production, low cost [18], high conductivity, chemical stability, and catalytic activity [19,20]. They have a wide range of applications in biomedicine and are commonly coupled with biomaterials to provide bactericidal effects [21]. By attaching to peptidoglycans, AgNPs can permeate bacteria membranes, causing structural alterations, increased membrane permeability, and, eventually, death [21]. AgNPs can also interact with bacterial proteins through this mechanism, inhibiting DNA replication and, consequently, bacterial growth [22].

A few different types of starches can be utilized to make scaffolds and biomaterials. They are derived from many plant sources and have varying compositions and properties that are determined by growing circumstances, area, harvest season, and climate [10,23–27]. Commercial starches made from wheat, corn, potato, rice, and cassava have already been extensively explored and are widely exploited in the industry [28]. Searching for novel forms of local starch sources in Brazil would be critical, given their importance and the differences in their qualities.

Jackfruit (*Artocarpus heterophyllus*) provides a different type of starch, showing potential among starch sources. The high amylose concentration, low gelatinization temperature, and small gelatinization enthalpy change of jackfruit starch make it a promising starch resource [27,29,30]. However, additional research is still necessary.

In this study, we synthesized a jackfruit (*Artocarpus heterophyllus*) starch-based scaffold loaded with AgNPs and tested its physicochemical, thermal, morphological, and cytotoxic properties for biomedical applications. The production of such scaffolds utilizing readily accessible, inexpensive, and domestic starch sources was another primary objective of this study.

2. Materials and Methods

2.1. Chemicals

The jackfruit used for starch extraction was obtained from the local market of Campina Grande, Paraiba, Brazil. All chemical reagents were of analytical grade. Silver nitrate ($AgNO_3$), tribasic sodium citrate dihydrate ($Na_3C_6H_5O_7.2H_2O$), and hydrogen peroxide 35% (H_2O_2) were purchased from Neon. Sodium borohydride ($NaBH_4$), and glycerol (≥99%) were from Sigma-Aldrich. The aqueous solutions were prepared with ultrapure water (18.2 $m\Omega.cm^{-1}$), obtained from a GEHAKA Master System MS2000 System.

2.2. Starch extraction from jackfruit seed endocarp

The starch extraction method was adopted from Perez, *et al.* [31]. In the first stage, jackfruit seeds were washed, peeled, and crushed in a blender until a thick and homogenous mass was obtained, adding water in a 1:4 (m/v) ratio. The paste was filtered through organza bags (100 mesh). The filtered starch suspension was decanted for 24 hours in a refrigerated atmosphere at 5 °C. The floating portion was removed, and the starch suspended in water was again decanted. This suspension and settling procedure were repeated until a white starch color was acquired. Following this, the starch was lyophilized (for 48 hours) and sieved to 200 mesh.

2.3. Synthesis of AgNPs

AgNPs were synthesized through the chemical reduction method described by Zhang, *et al.* [32]. Initially, 30 mL of ultrapure water was transferred to a beaker and magnetic stirring (500 rpm) was performed at room temperature (25 °C). The system was then filled with 30 µL of silver nitrate (0.1 $mol.L^{-1}$), 1.5 mL of sodium citrate (0.9 $mmol.L^{-1}$), 60 µL of hydrogen peroxide (35%), and 200 µL of sodium borohydride (90 $mmol.L^{-1}$). After adding sodium borohydride, the magnetic stirring was increased to 1150 rpm for 3

 doi:10.20944/preprints202211.0092.v1

minutes, the period required for forming AgNPs. Our earlier study [33] provides more information on the effects of mixing intervals and variations in the volume and concentration of $NaBH_4$ and H_2O_2 on the size, dispersion, and stability of AgNPs.

2.4. Synthesis of starch jackfruit scaffold

The starch scaffold was obtained according to the methodology proposed by Perez, Bahnassey and Breene [31]. 7.5 g of starch and 2.5 mL of glycerol were first added to a beaker containing 250 mL of ultrapure water while magnetic stirring (300 rpm) was performed at 85 °C. The starch solution was then cooled to room temperature (25 °C), transferred to Petri dishes, and frozen (24 hours), defrosted (2 hours), frozen (24 hours), and lyophilized.

2.5. Synthesis of Starch-AgNPs scaffold

The starch-AgNPs scaffold was developed using the same process as the starch jackfruit scaffold, with a few modifications. After cooling to room temperature, 12.5 mL of the AgNPs solution (1×10^{-3} mol.L^{-1}) was added, followed by freezing (24 hours), defrosting (2 hours), freezing (24 hours), and lyophilizing.

2.6. Characterizations

2.6.1. Characterization of the silver nanoparticles (AgNPs)

UV-Vis spectroscopy was used to confirm the synthesis of AgNPs. A Bomem-Michelson spectrophotometer, model MB-102, was used to scan in the wavelength range of 250-1100 nm. The spectrums were collected using quartz cuvettes with a 10 mm optical path.

The size, polydispersity, and stability of nanoparticles were determined using dynamic light scattering (DLS) and Zeta potential (PZ) techniques. The analyses were carried out on a Brookhaven Zeta ZetaPals Instrument. The tests were performed at room temperature without diluting the samples, with a scattering angle of 90°, laser wavelength of 632.8 nm (He-Ne), average viscosity of 0.887 mPa.s, and refractive index of 1.330. All measurements were taken three times.

The AgNPs morphology was investigated using a field emission scanning electron microscope (FE-SEM, Hitachi model S4700EI), operating at a voltage of 15 kV. AgNPs were diluted in ultrapure water at a ratio of 1:10 and coated with platinum.

2.6.2. Scaffolds characterization

X-ray diffraction (XRD) was used to prove the inclusion of AgNPs in the starch-AgNPs composite and to verify the crystallinity of the starch. The experiment was carried out on a Shimadzu XRD-7000 with CuKα radiation (1.5418), 40 kV, and 30 mA current, in the interval of 10-80° and a resolution of 2°/min. The General System Analyzer Structure (GSAS II) program was utilized for Rietveld refinement.

FTIR spectroscopy was employed to identify the vibration bands of starch and to assess the interaction between starch and AgNPs. The analysis was carried out on a Perkin Elmer Spectrum 400 device in the range of 4000-650 cm^{-1} with a resolution of 4 cm^{-1} in diffuse reflectance mode for 32 scans at room temperature (25 °C) using an attenuated total reflectance (ATR) accessory equipped with zinc selenium (ZnSe) crystal.

To analyze the existence of AgNPs in the scaffold, evaluate morphological changes following AgNPs incorporation, and identify the starch microstructure, scanning electron microscopy coupled with energy-dispersive X-ray spectroscopy (SEM-EDS, HITACHI model TM-1000) was used. All images were taken from uncoated samples at a 15 kV accelerating voltage, 1 mm depth of focus, 30 nm resolution, low vacuum, and variable pressure (1 to 270 Pa). At the same conditions, EDS analyses were performed on an EDS Quantax 50 XFlash Bruker. Image processing was carried out using the Quantax 50 program.

 doi:10.20944/preprints202211.0092.v1

The thermal stability of the starch and starch-AgNPs scaffolds was evaluated using differential scanning calorimetry (DSC). A PerkinElmer DSC, model 8500, was employed in a temperature range of 25-300 °C, a heating rate of 10 °C/min, in a nitrogen atmosphere, and a flow rate of 20 mL/min. Alumina crucible and a sample mass of 3.00 ± 0.05 mg were used.

The cytotoxicity assessment was performed according to the direct contact method described in ISO 10993-5:2009 [34] and ISO 10993-12:1998 [35]. Initially, 0.5 g of scaffolds were weighed and sterilized for 30 minutes via UV radiation. Next, the extracts were prepared by submerging the scaffolds in 1.25 mL of PBS solution (0.05 M) for 24 hours. Then, 100 µL/well of L929 cells suspension were seeded in 96-well plates and incubated for 24 hours at 37 °C ± 1 °C under 5% ± 1% CO_2 atmosphere. After cultivation, 50 µL of the medium extracted from the samples was added and the cells were incubated for another 24 hours. Finally, the cytotoxicity assay was conducted by the MTT method.

After the incubation time, the culture medium was removed and 100 µL of MTT solution (5 $mg.mL^{-1}$) was added and the plates were incubated under the same conditions for another 4 hours. The cells were then treated with 100 µL of DMSO to dissolve the formazan crystals. Plates were read by the optical density method on the PerkinElmer Victor X3 microplate reader at 570 nm with 650 nm reference filters. Latex sheets and high-density polyethylene (HDPE) were used as positive and negative controls, respectively.

3. Results and Discussion

3.1. Characterization of the silver nanoparticles (AgNPs)

The UV-Vis spectrum of the AgNPs colloidal solution is shown in Figure 1A. Three absorption bands were found in the UV-Vis analysis. According to the Schatz calculation, the first band at 333 nm corresponds to out-of-plane quadrupole resonance; the second shoulder-shaped band around 465 nm indicates dipole resonances characteristic of triangular nanoparticles [36]; and the third band with maximum absorption at 744 nm resembles the plasmonic surface characteristic of the resonance band of almost perfect triangular nanoparticles [36,37]. According to Mie's hypothesis, anisotropic particles should be present because they have three absorption bands [37,38]. Furthermore, the colloidal solution of AgNPs acquires a blue color after synthesis, which can be attributed to the plasmonic excitation of the surface of triangular-shaped nanoparticles (nanoplates) [39,40].

The nanoparticles in the DLS result (Inset of Figure 1A) had an average size of 33.27 nm and a polydispersity index (PDI) of 0.205, which is typical of monodisperse solutions (0.300), which range from 0 to 1. As a result, the smaller the value, the more monodisperse the colloid [41]. PZ findings revealed AgNPs with a surface charge of -33.39 mV, confirming stable AgNP production [39]. Additionally, Figure 1B is an FE-SEM micrograph showing the formation of nano-sized, anisotropic, monodisperse silver particles.

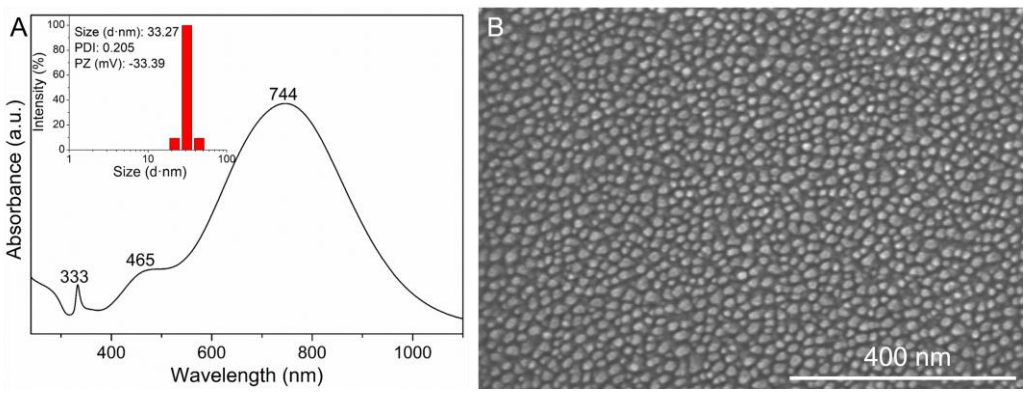

Figure 1. (A) UV-Vis spectrum of AgNPs colloidal solution. Inset: Size distribution of AgNPs measured by the DLS. (B) FE-SEM micrograph showing the formation of nano-sized, anisotropic, monodisperse silver particles.

 doi:10.20944/preprints202211.0092.v1

3.2. Morphological characterization

SEM micrographs of jackfruit starch granules, starch scaffold, and starch-AgNPs scaffold are shown in Figure 2A-F. The starch granules (Figures 2A and 2B) had a rounded irregular bell shape with cuts on their surface, which are typical of this type of starch [42]. The granules ranged in size from 4-6 µm. Dutta, *et al.* [43] and Zhang, Zhu, He, Tan and Kong [29] found similar results.

SEM micrographs of the starch scaffold and starch-AgNPs scaffold shown in Figures 2C, 2D, 2E, and 2F revealed that both scaffolds had a porous structure created by well-defined pores and arranged with high interconnectivity. Water evaporation during the lyophilization process resulted in a significant level of porosity [44,45]. It appears that adding AgNPs roughens the surface of the scaffold, facilitating cell attachment and proliferation [46]. The incorporation of metallic nanoparticles into the starch polymer matrix has been shown to modify the interactions between starch and glycerol [47,48], increasing its compactness and roughness.

The EDS analysis revealed the presence of AgNPs in the scaffold (Figure 2G). Starch was associated with levels of 59.4% carbon and 33.2% oxygen. The silver ions in the nanoparticles were responsible for the 5.4% silver content. The findings of Li, *et al.* [49] and Vaidhyanathan, *et al.* [50] are consistent with these results.

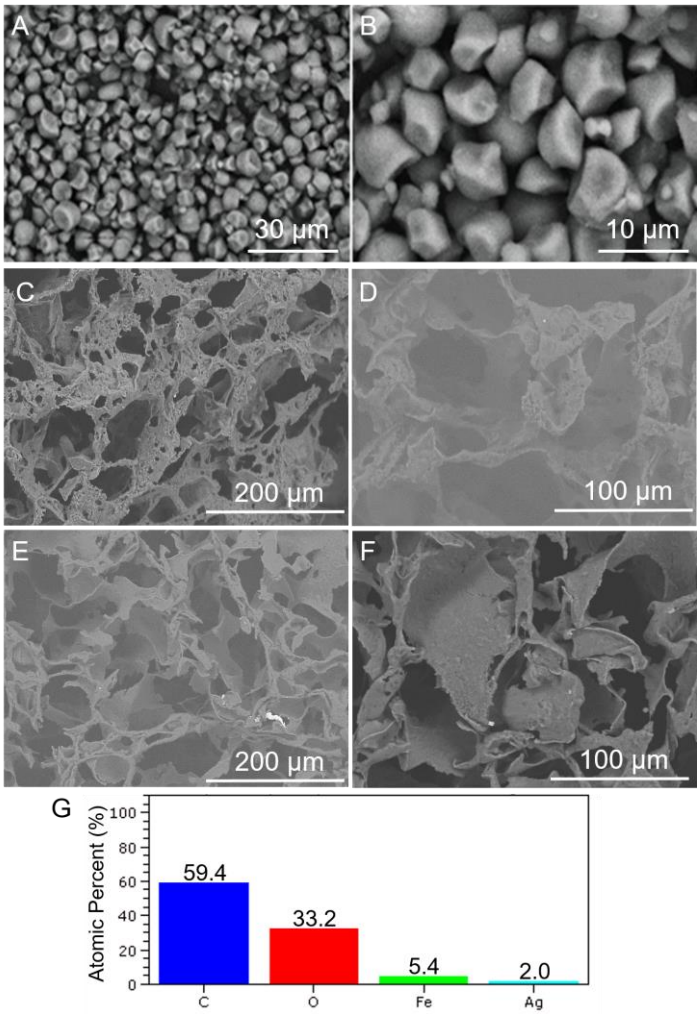

Figure 2. SEM micrographs of (A) and (B) jackfruit starch granules; (C) and (D) Cross-section of starch scaffold; and (E) and (F) starch-AgNPs scaffold. (G) EDS analysis of the starch-AgNPs scaffold.

 doi:10.20944/preprints202211.0092.v1

3.3. Phase analysis

Figure 3 depicts the XRD pattern of jackfruit starch, starch scaffold, and starch-AgNPs scaffold. According to Figure 3B, the starch scaffold exhibited amorphous polymer structures with a crystallinity of 16.95% according to the Rietveld refinement; diffraction peaks positioned at 15.86°, 17.38°, 21,04°, 22.94°, 23.88°, and 28.88°; confirming the crystalline structure of type A [51,52]. These peaks in the scaffold are identical to the peaks in the starch diffractogram (Figure 3A), although with lower intensity, as explained by Pozo, Rodríguez-Llamazares, Bouza, Barral, Castaño, Müller and Restrepo [52] and Dutta, *et al.* [53].

After adding AgNPs into the scaffold (Figure 3C), the crystallinity increased to 33.88%, representing a 16.93% increase over the scaffold without AgNPs. It has been shown that the presence of AgNPs leads to a higher degree of crystallinity in polyimide films [54]. Furthermore, the starch-AgNPs scaffold exhibited four diffraction peaks at 37.80°, 44.02°, 64.36°, and 77.50°, which corresponded to the planes (111), (200), (220), and (311) and correlated to the face-centered cubic structure of metallic silver (JCPDS file No. 03-0921). This validated the inclusion of AgNPs in the scaffold [55–57].

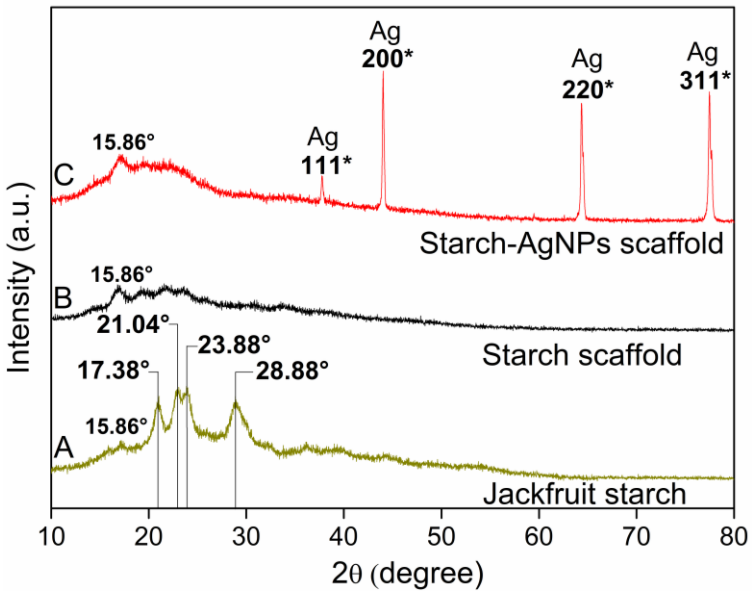

Figure 3. XRD pattern of (A) starch jackfruit, (B) starch scaffold and (C) starch-AgNPs scaffold.

3.4. Scaffold chemistry

The FTIR spectra of starch, starch scaffold, and starch-AgNPs scaffold are shown in Figure 4. The vibration bands in the jackfruit starch spectrum (Figure 4A) represent features of the molecular deformations present in the starch molecules. Stretching and angular deformation of –OH and C–O–H bonds are responsible for the bands localizated at 3400 and 1650 cm^{-1}, respectively. The symmetrical and asymmetrical stretches of –C–H are represented by vibration bands at 2926 and 2897 cm^{-1}, respectively. The C–O–H bonds are represented by the bands 1460-1400 cm^{-1}. Absorptions at 1340 and 1024 cm^{-1} are due to –C–OH group deformations. Vibration modes associated with –C–C–H bonds were detected at 1418, 1205, and 1080 cm^{-1}, whereas C–O, C–O–C, and C–C stretches correspond to 1153, 1107, and 933 cm^{-1} bands, which are typical of the vibration modes associated with pyranose rings found in natural polysaccharides [58–61]. Therefore, all these bands could be related to jackfruit starch bonds.

The FTIR spectra of the starch (Figure 4B) and starch-AgNPs (Figure 4C) scaffolds matched the starch jackfruit spectrum very well. Such behavior shows that the interaction of the AgNPs with the starch is physical rather than chemical [62,63]. This suggests that

 doi:10.20944/preprints202211.0092.v1

while AgNPs are present in the scaffold (as shown by the XRD and EDS data), they do not chemically interact to the starch polymer chains.

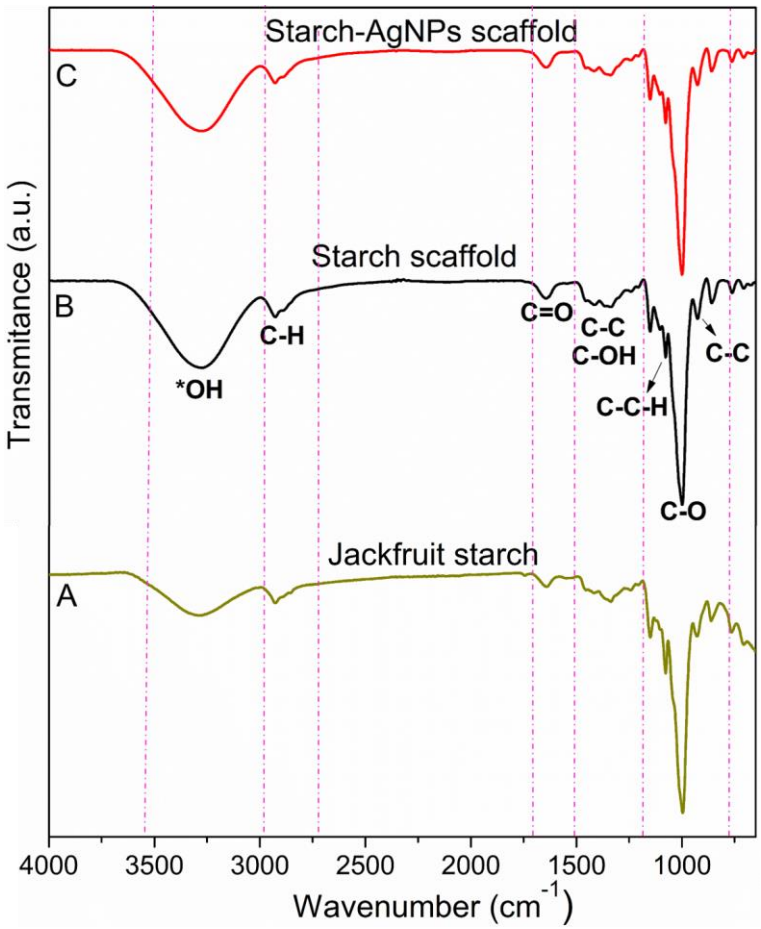

Figure 4. FTIR spectra of (A) jackfruit starch, (B) starch scaffold and (C) starch-AgNPs scaffold.

3.5. Thermal analysis

Figure 5 depicts the thermograms of the starch and starch-AgNPs scaffolds, which display three endothermic peaks. The first refers to starch gelatinization, which has a gelatinization temperature of 81.3 and 71.3 °C in the starch and starch-AgNPs scaffolds, respectively; the second peak, at temperatures of 110.2 °C and 105.8 °C in the starch scaffold and starch-AgNPs scaffold, can be attributed to the gelatinization of the amylose present in the starch, which is complexed by lipid [29,64–66]. The melting temperature (T_m, third peak) of the starch increases from 146.3 °C to 185.2 °C with AgNPs incorporation. This peak is caused by the melting of crystalline starch domains that have been reorganized during retrogradation [67].

The results reveal that after incorporating AgNPs, the gelatinization temperatures of starch and amylose decrease while the T_m rises. There is evidence that AgNPs and other metallic nanoparticles have a greater effect on the T_m than they do on changing the initial degradation temperatures, as was the case for the gelatinization temperatures [63,68]. The increase in T_m is explained by the fact that AgNPs are more heat-stable [63,69]. Shameli, *et al.* [70] reported similar results, observing an 18% increase in the enthalpy of starch-AgNPs composite films. Heat stability was similarly enhanced when AgNPs were included in gelatin films and sugar palm starch biocomposites, as observed by Kanmani and Rhim [71] and Rozilah *et al.* [69], respectively.

Preprints (www.preprints.org) | NOT PEER-REVIEWED | Posted: 4 November 2022 doi:10.20944/preprints202211.0092.v1

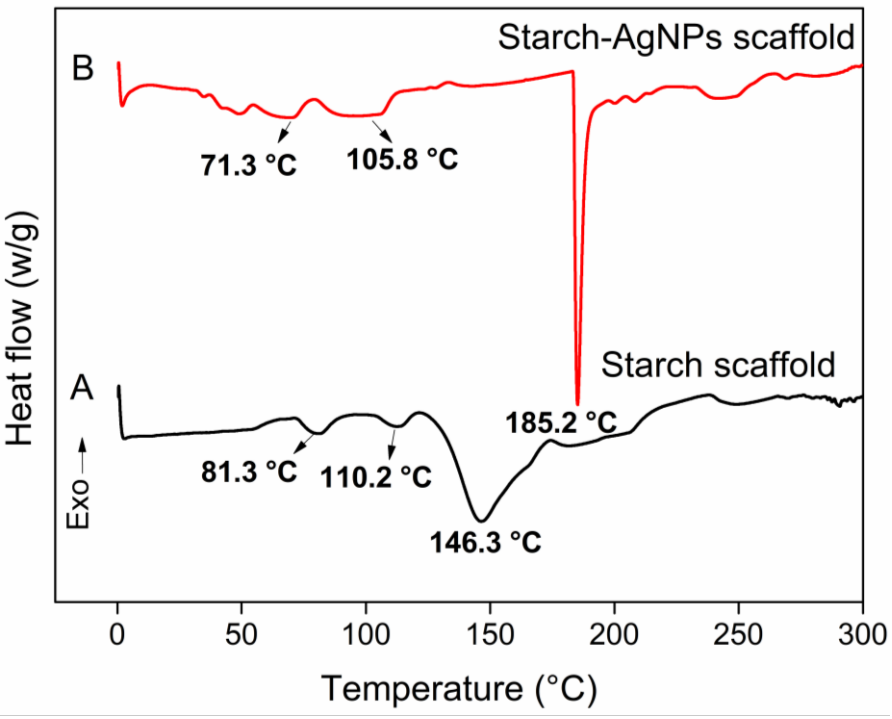

Figure 5. DSC analysis of (A) starch scaffold and (B) starch-AgNPs scaffold.

3.6. Cytotoxicity analysis

Figure 6 demonstrates that the cell viability values of both scaffolds, one without AgNPs and one with, were 80.2% and 80.3%, respectively. Also, adding AgNPs did not result in any reduction in the viability of the cells, which suggests that AgNPs do not have any cytotoxic effects. The veracity of the data was confirmed by the fact that the negative control showed a hundred percent cell proliferation. According to ISO 10993-5, if the material has a value that is lower than 70%, it is considered to have a toxic effect [34]. Both scaffolds exhibited cell survival values higher than 70%, demonstrating that the jackfruit starch scaffold loaded with AgNPs is not toxic to L929 cells. Therefore, it is appropriate for application as a biomaterial in treating various conditions, such as wounds.

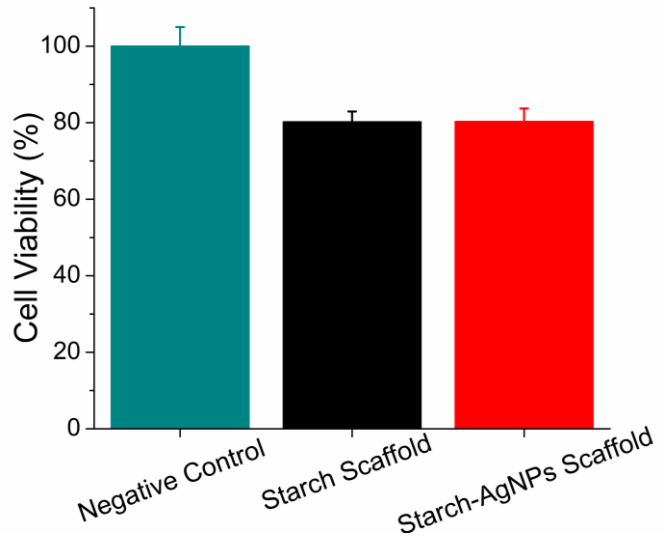

Figure 6. Cytotoxicity of negative control, starch scaffold and starch-AgNPs scaffold obtained by the MTT method.

 doi:10.20944/preprints202211.0092.v1

4. Conclusions

In this study, we investigated the impact of incorporating silver nanoparticles (AgNPs) into a Brazilian jackfruit (*Artocarpus heterophyllus*) starch-based scaffold by analyzing its chemical, physical, thermal, and morphological characteristics. The chemical reduction technique yielded monodisperse, isotropic, and stable AgNPs with a size of 33.27 nm. The presence of AgNPs in the starch scaffold was verified by EDS and XRD analyses. The FTIR spectra of jackfruit starch and starch-AgNPs scaffolds were identical, suggesting that the interaction of AgNPs with starch was purely physical. SEM revealed the scaffolds to have a very porous three-dimensional structure. AgNPs inclusion maintained the scaffold's porosity while increasing its surface roughness and crystallinity, all conducive to enhancing biological responses. In conclusion, the crystallinity, roughness, and melting temperature of the starch jackfruit scaffold were all improved by the addition of AgNPs. The scaffold could be developed using AgNPs to better survive temperature changes and demonstrate stronger biological interactions. The L929 cell survival rate was greater than 70% for both scaffolds, confirming that the scaffold loaded with AgNPs is non-toxic to L929 cells and hence is clinically relevant for treating, i.e., wounds. These findings have implications for a wide variety of starch-based scaffolds. The next stage of our investigation will involve applying this strategy to adding AgNPs and fine-tuning the biological characteristics of the scaffold.

Author Contributions: Conceptualization, data curation, investigation, methodology and writing – original draft, J.F.B.R.; Funding acquisition, V.S.A.; Data curation and visualization, R.P.M.; Investigation, data curation and methodology, G.B.C.B.; Project administration and supervision, M.R.O.P.; Resources, M.V.L.F.; Visualization and writing – review & editing, M.M. All authors have read and agreed to the published version of the manuscript.

Funding: This research received no external funding.

Data Availability Statement: Not applicable.

Acknowledgments: The authors would like to acknowledge Coordination for the Improvement of Higher Education Personnel (CAPES), the National Council for Scientific and Technological Development (CNPq), the Northeast Laboratory for Evaluation and Development of Biomaterials (CERTBIO), and the Federal University of Campina Grande (UFCG).

Conflicts of Interest: The authors declare no conflict of interest.

References

1. Berner, A.; Woodruff, M.; Lam, C.; Arafat, M.; Saifzadeh, S.; Steck, R.; Ren, J.; Nerlich, M.; Ekaputra, A.K.; Gibson, I. Effects of scaffold architecture on cranial bone healing. International journal of oral and maxillofacial surgery 2014, 43, 506-513.
2. Cui, Z.; Nelson, B.; Peng, Y.; Li, K.; Pilla, S.; Li, W.-J.; Turng, L.-S.; Shen, C. Fabrication and characterization of injection molded poly (ε-caprolactone) and poly (ε-caprolactone)/hydroxyapatite scaffolds for tissue engineering. Materials Science and Engineering: C 2012, 32, 1674-1681.
3. Silva, M.C.; Nascimento, I.; Ribeiro, V.d.S.; Fook, M.V.L. Avaliação do método de obtenção de scaffolds quitosana/curcumina sobre a estrutura, morfologia e propriedades térmicas. Matéria (Rio de Janeiro) 2016, 21, 560-568.
4. Movahedi, M.; Asefnejad, A.; Rafienia, M.; Khorasani, M.T. Potential of novel electrospun core-shell structured polyurethane/starch (hyaluronic acid) nanofibers for skin tissue engineering: In vitro and in vivo evaluation. International journal of biological macromolecules 2020, 146, 627-637.
5. Ghavimi, M.A.; Negahdari, R.; Bani Shahabadi, A.; Sharifi, S.; Kazeminejad, E.; Shahi, S.; Maleki Dizaj, S. Preparation and study of starch/collagen/polycaprolactone nanofiber scaffolds for bone tissue engineering using electrospinning technique. Eurasian Chemical Communications 2020, 2, 122-127.
6. Grabska-Zielińska, S.; Sionkowska, A.; Reczyńska, K.; Pamuła, E. Physico-chemical characterization and biological tests of collagen/silk fibroin/chitosan scaffolds cross-linked by dialdehyde starch. Polymers 2020, 12, 372.
7. Taherimehr, M.; Bagheri, R.; Taherimehr, M. In-vitro Evaluation of Thermoplastic Starch/Beta-tricalcium Phosphate Nanobiocomposite in Bone Tissue Engineering. Ceramics International 2021.
8. Jiang, T.; Duan, Q.; Zhu, J.; Liu, H.; Yu, L. Starch-based biodegradable materials: Challenges and opportunities. Advanced Industrial and Engineering Polymer Research 2020, 3, 8-18.

9. El-Sheikh, M.A. New technique in starch nanoparticles synthesis. Carbohydr Polym 2017, 176, 214-219, doi:10.1016/j.carbpol.2017.08.033.
10. Batool, S.; Hussain, Z.; Niazi, M.B.K.; Liaqat, U.; Afzal, M. Biogenic synthesis of silver nanoparticles and evaluation of physical and antimicrobial properties of Ag/PVA/starch nanocomposites hydrogel membranes for wound dressing application. Journal of Drug Delivery Science and Technology 2019, 52, 403-414.
11. Irani, M.; Razavi, S.M.; Abdel-Aal, E.-S.M.; Hucl, P.; Patterson, C.A. Viscoelastic and textural properties of canary seed starch gels in comparison with wheat starch gel. International journal of biological macromolecules 2019, 124, 270-281.
12. Ashraf, R.; Sofi, H.S.; Malik, A.; Beigh, M.A.; Hamid, R.; Sheikh, F.A. Recent trends in the fabrication of starch nanofibers: electrospinning and non-electrospinning routes and their applications in biotechnology. Applied biochemistry and biotechnology 2019, 187, 47-74.
13. Luo, K.; Adra, H.J.; Kim, Y.-R. Preparation of starch-based drug delivery system through the self-assembly of short chain glucans and control of its release property. Carbohydrate Polymers 2020, 243, 116385.
14. Nallasamy, P.; Ramalingam, T.; Nooruddin, T.; Shanmuganathan, R.; Arivalagan, P.; Natarajan, S. Polyherbal drug loaded starch nanoparticles as promising drug delivery system: Antimicrobial, antibiofilm and neuroprotective studies. Process Biochemistry 2020, 92, 355-364.
15. El-Sheikh, M. A novel photosynthesis of carboxymethyl starch-stabilized silver nanoparticles. The Scientific World Journal 2014, 2014.
16. Wawro, D.; Bodek, A.; Bodek, K.H. Starch Film as a Carrier of a Model Drug Substance from the Group of Non-Steroidal Anti-Inflammatory Drugs. Fibres & Textiles in Eastern Europe 2018.
17. Jalal, M.; Ansari, M.A.; Alzohairy, M.A.; Ali, S.G.; Khan, H.M.; Almatroudi, A.; Raees, K. Biosynthesis of silver nanoparticles from oropharyngeal candida glabrata isolates and their antimicrobial activity against clinical strains of bacteria and fungi. Nanomaterials 2018, 8, 586.
18. Luu, T.; Cao, X.T.; Nguyen, V.; Pham, N.L.; Nguyen, H.L.; Nguyen, C.T. Simple controlling ecofriendly synthesis of silver nanoparticles at room temperature using lemon juice extract and commercial rice vinegar. Journal of Nanotechnology 2020, 2020.
19. Fernando, I.; Zhou, Y. Impact of pH on the stability, dissolution and aggregation kinetics of silver nanoparticles. Chemosphere 2019, 216, 297-305.
20. Ajitha, B.; Reddy, Y.A.K.; Jeon, H.-J.; Ahn, C.W. Synthesis of silver nanoparticles in an eco-friendly way using Phyllanthus amarus leaf extract: Antimicrobial and catalytic activity. Advanced Powder Technology 2018, 29, 86-93.
21. Bapat, R.A.; Joshi, C.P.; Bapat, P.; Chaubal, T.V.; Pandurangappa, R.; Jnanendrappa, N.; Gorain, B.; Khurana, S.; Kesharwani, P. The use of nanoparticles as biomaterials in dentistry. Drug discovery today 2019, 24, 85-98.
22. Seth, D.; Choudhury, S.R.; Pradhan, S.; Gupta, S.; Palit, D.; Das, S.; Debnath, N.; Goswami, A. Nature-inspired novel drug design paradigm using nanosilver: efficacy on multi-drug-resistant clinical isolates of tuberculosis. Current microbiology 2011, 62, 715-726.
23. Aktürk, A.; Taygun, M.E.; Güler, F.K.; Goller, G.; Küçükbayrak, S. Fabrication of antibacterial polyvinylalcohol nanocomposite mats with soluble starch coated silver nanoparticles. Colloids and Surfaces A: Physicochemical and Engineering Aspects 2019, 562, 255-262.
24. Waghmare, V.S.; Wadke, P.R.; Dyawanapelly, S.; Deshpande, A.; Jain, R.; Dandekar, P. Starch based nanofibrous scaffolds for wound healing applications. Bioact Mater 2018, 3, 255-266.
25. Dai, L.; Zhang, J.; Cheng, F. Effects of starches from different botanical sources and modification methods on physicochemical properties of starch-based edible films. International journal of biological macromolecules 2019, 132, 897-905.
26. Zhang, D.; Mu, T.; Sun, H. Effects of starch from five different botanical sources on the rheological and structural properties of starch–gluten model doughs. Food research international 2018, 103, 156-162.
27. Zhang, Y.; Li, B.; Xu, F.; He, S.; Zhang, Y.; Sun, L.; Zhu, K.; Li, S.; Wu, G.; Tan, L. Jackfruit starch: Composition, structure, functional properties, modifications and applications. Trends in Food Science & Technology 2020.
28. Rolland-Sabaté, A.; Sanchez, T.; Buléon, A.; Colonna, P.; Ceballos, H.; Zhao, S.-S.; Zhang, P.; Dufour, D. Molecular and supra-molecular structure of waxy starches developed from cassava (Manihot esculenta Crantz). Carbohydrate Polymers 2013, 92, 1451-1462.
29. Zhang, Y.; Zhu, K.; He, S.; Tan, L.; Kong, X. Characterizations of high purity starches isolated from five different jackfruit cultivars. Food hydrocolloids 2016, 52, 785-794.
30. Zhang, Y.; Zhang, Y.; Xu, F.; Li, S.; Tan, L. Structural characterization of starches from Chinese jackfruit seeds (Artocarpus heterophyllus Lam). Food hydrocolloids 2018, 80, 141-148.
31. Perez, E.; Bahnassey, Y.; Breene, W. A simple laboratory scale method for isolation of amaranth starch. Starch-Stärke 1993, 45, 211-214.
32. Zhang, Q.; Li, N.; Goebl, J.; Lu, Z.; Yin, Y. A systematic study of the synthesis of silver nanoplates: is citrate a "magic" reagent? Journal of the American Chemical Society 2011, 133, 18931-18939.
33. Rodrigues, J.F.B.; Brandão, P.E.d.S.; Guimarães, P.Q.; Pinto, M.R.d.O.; Wellen, R.M.R.; Fook, M.V.L. Aplicação de método estatístico no estudo da influência do peróxido de hidrogênio e do borohidreto de sódio na síntese de nanoparticulas de prata (AGNPS). Matéria (Rio de Janeiro) 2019, 24.
34. Organization, I.S. ISO 10993-5: 2009. Biological evaluation of medical devices–Part 5: Tests for in vitro cytotoxicity. 2009.

35. 35.Standardization, I. ISO 10993-12: Biological Evaluation of Medical Devices—Part 12: Sample Preparation and Reference Materials. Geneva: International Organization for Standardization (ISO) 2012.
36. Farooq, S.; Nunes, F.D.; de Araujo, R.E. Optical properties of silver nanoplates and perspectives for biomedical applications. Photonics and Nanostructures-Fundamentals and Applications 2018, 31, 160-167.
37. Rycenga, M.; Cobley, C.M.; Zeng, J.; Li, W.; Moran, C.H.; Zhang, Q.; Qin, D.; Xia, Y. Controlling the synthesis and assembly of silver nanostructures for plasmonic applications. Chemical reviews 2011, 111, 3669-3712.
38. Huang, G.; He, J.; Zhang, X.; Feng, M.; Tan, Y.; Lv, C.; Huang, H.; Jin, Z. Applications of Lambert-Beer law in the preparation and performance evaluation of graphene modified asphalt. Construction and Building Materials 2021, 273, 121582.
39. Rodrigues, J.; Junior, E.; Oliveira, K.; Wellen, M.; Simões, S.; Fook, M. Multivariate Model Based on UV-Vis Spectroscopy and Regression in Partial Least Squares for Determination of Diameter and Polydispersity of Silver Nanoparticles in Colloidal Suspensions. Journal of Nanomaterials 2020, 2020.
40. Panzarasa, G. Just what is it that makes silver nanoprisms so different, so appealing? Journal of Chemical Education 2015, 92, 1918-1923.
41. Mahl, D.; Diendorf, J.; Meyer-Zaika, W.; Epple, M. Possibilities and limitations of different analytical methods for the size determination of a bimodal dispersion of metallic nanoparticles. Colloids and Surfaces A: Physicochemical and Engineering Aspects 2011, 377, 386-392, doi:10.1016/j.colsurfa.2011.01.031.
42. Kittipongpatana, O.S.; Kittipongpatana, N. Preparation and physicochemical properties of modified jackfruit starches. LWT - Food Science and Technology 2011, 44, 1766-1773, doi:10.1016/j.lwt.2011.03.023.
43. Dutta, H.; Paul, S.K.; Kalita, D.; Mahanta, C.L. Effect of acid concentration and treatment time on acid-alcohol modified jackfruit seed starch properties. Food Chem 2011, 128, 284-291, doi:10.1016/j.foodchem.2011.03.016.
44. Chen, Z.; Yan, X.; Yin, S.; Liu, L.; Liu, X.; Zhao, G.; Ma, W.; Qi, W.; Ren, Z.; Liao, H. Influence of the pore size and porosity of selective laser melted Ti6Al4V ELI porous scaffold on cell proliferation, osteogenesis and bone ingrowth. Materials Science and Engineering: C 2020, 106, 110289.
45. Hao, Z.; Song, Z.; Huang, J.; Huang, K.; Panetta, A.; Gu, Z.; Wu, J. The scaffold microenvironment for stem cell based bone tissue engineering. Biomaterials Science 2017, 5, 1382-1392.
46. Mehrabani, M.G.; Karimian, R.; Mehramouz, B.; Rahimi, M.; Kafil, H.S. Preparation of biocompatible and biodegradable silk fibroin/chitin/silver nanoparticles 3D scaffolds as a bandage for antimicrobial wound dressing. International journal of biological macromolecules 2018, 114, 961-971.
47. Francis, D.V.; Thaliyakattil, S.; Cherian, L.; Sood, N.; Gokhale, T. Metallic Nanoparticle Integrated Ternary Polymer Blend of PVA/Starch/Glycerol: A Promising Antimicrobial Food Packaging Material. Polymers 2022, 14, 1379.
48. Abdullah, Z.W.; Dong, Y. Biodegradable and Water Resistant Poly(vinyl) Alcohol (PVA)/Starch (ST)/Glycerol (GL)/Halloysite Nanotube (HNT) Nanocomposite Films for Sustainable Food Packaging. Frontiers in Materials 2019, 6, doi:10.3389/fmats.2019.00058.
49. Li, J.; Li, L.; Zhou, J.; Zhou, Z.; Wu, X.-l.; Wang, L.; Yao, Q. 3D printed dual-functional biomaterial with self-assembly micro-nano surface and enriched nano argentum for antibacterial and bone regeneration. Applied Materials Today 2019, 17, 206-215.
50. Vaidhyanathan, B.; Vincent, P.; Vadivel, S.; Karuppiah, P.; AL-Dhabi, N.A.; Sadhasivam, D.R.; Vimalraj, S.; Saravanan, S. Fabrication and Investigation of the Suitability of Chitosan-Silver Composite Scaffolds for Bone Tissue Engineering Applications. Process Biochemistry 2021, 100, 178-187.
51. Dome, K.; Podgorbunskikh, E.; Bychkov, A.; Lomovsky, O. Changes in the crystallinity degree of starch having different types of crystal structure after mechanical pretreatment. Polymers 2020, 12, 641.
52. Pozo, C.; Rodríguez-Llamazares, S.; Bouza, R.; Barral, L.; Castaño, J.; Müller, N.; Restrepo, I. Study of the structural order of native starch granules using combined FTIR and XRD analysis. Journal of Polymer Research 2018, 25, 1-8.
53. 53.Dutta, S.; Dutta, H.; Devi, D. Development of Novel 2D Composites of Silk Sericin and Rice Starch and Application as Bio-Compatible Scaffold for Cell Culturing. Starch-Stärke 2018, 70, 1700270.
54. Triambulo, R.E.; Cheong, H.-G.; Lee, G.-H.; Yi, I.-S.; Park, J.-W. A transparent conductive oxide electrode with highly enhanced flexibility achieved by controlled crystallinity by incorporating Ag nanoparticles on substrates. Journal of Alloys and Compounds 2015, 620, 340-349.
55. Siddiqui, M.R.H.; Adil, S.; Nour, K.; Assal, M.; Al-Warthan, A. Ionic liquid behavior and high thermal stability of silver chloride nanoparticles: synthesis and characterization. Arabian Journal of Chemistry 2013, 6, 435-438.
56. Ullah, I.; Shinwari, Z.K.; Khalil, A.T. Investigation of the cytotoxic and antileishmanial effects of Fagonia indica L. extract and extract mediated silver nanoparticles (AgNPs). Pak J Bot 2017, 49, 1561-1568.
57. Adil, M.; Khan, T.; Aasim, M.; Khan, A.A.; Ashraf, M. Evaluation of the antibacterial potential of silver nanoparticles synthesized through the interaction of antibiotic and aqueous callus extract of Fagonia indica. AMB Express 2019, 9, 1-12.
58. Machado, B.A.S.; Nunes, I.L.; Pereira, F.V.; Druzian, J.I. Desenvolvimento e avaliação da eficácia de filmes biodegradáveis de amido de mandioca com nanocelulose como reforço e com extrato de erva-mate como aditivo antioxidante. Ciência Rural 2012, 42, 2085-2091.
59. Al-Hassan, A.; Norziah, M. Starch–gelatin edible films: Water vapor permeability and mechanical properties as affected by plasticizers. Food Hydrocolloids 2012, 26, 108-117.

60. Warren, F.J.; Gidley, M.J.; Flanagan, B.M. Infrared spectroscopy as a tool to characterise starch ordered structure—a joint FTIR–ATR, NMR, XRD and DSC study. Carbohydrate polymers 2016, 139, 35-42.
61. Nayak, A.K.; Pal, D.; Santra, K. Screening of polysaccharides from tamarind, fenugreek and jackfruit seeds as pharmaceutical excipients. International journal of biological macromolecules 2015, 79, 756-760.
62. Wu, Z.; Hong, Y. Combination of the silver–ethylene interaction and 3D printing to develop antibacterial superporous hydrogels for wound management. ACS applied materials & interfaces 2019, 11, 33734-33747.
63. Ji, N.; Liu, C.; Zhang, S.; Xiong, L.; Sun, Q. Elaboration and characterization of corn starch films incorporating silver nanoparticles obtained using short glucan chains. LWT-Food Science and Technology 2016, 74, 311-318.
64. Madruga, M.S.; de Albuquerque, F.S.M.; Silva, I.R.A.; do Amaral, D.S.; Magnani, M.; Neto, V.Q. Chemical, morphological and functional properties of Brazilian jackfruit (Artocarpus heterophyllus L.) seeds starch. Food chemistry 2014, 143, 440-445.
65. Zhang, Y.; Zhang, Y.; Xu, F.; Wu, G.; Tan, L. Molecular structure of starch isolated from jackfruit and its relationship with physicochemical properties. Scientific reports 2017, 7, 1-12.
66. Guo, K.; Lin, L.; Fan, X.; Zhang, L.; Wei, C. Comparison of structural and functional properties of starches from five fruit kernels. Food chemistry 2018, 257, 75-82.
67. Almasi, H.; Ghanbarzadeh, B.; Entezami, A.A. Physicochemical properties of starch–CMC–nanoclay biodegradable films. International journal of biological macromolecules 2010, 46, 1-5.
68. Hosseini, S.N.; Pirsa, S.; Farzi, J. Biodegradable nano composite film based on modified starch-albumin/MgO; antibacterial, antioxidant and structural properties. Polymer Testing 2021, 97, 107182, doi:https://doi.org/10.1016/j.polymertesting.2021.107182.
69. Rozilah, A.; Jaafar, C.N.A.; Sapuan, S.M.; Zainol, I.; Ilyas, R.A. The Effects of Silver Nanoparticles Compositions on the Mechanical, Physiochemical, Antibacterial, and Morphology Properties of Sugar Palm Starch Biocomposites for Antibacterial Coating. Polymers (Basel) 2020, 12, doi:10.3390/polym12112605.
70. Shameli, K.; Ahmad, M.B.; Yunus, W.M.Z.W.; Ibrahim, N.A.; Rahman, R.A.; Jokar, M.; Darroudi, M. Silver/poly (lactic acid) nanocomposites: preparation, characterization, and antibacterial activity. International journal of nanomedicine 2010, 5, 573.
71. Kanmani, P.; Rhim, J.-W. Physicochemical properties of gelatin/silver nanoparticle antimicrobial composite films. Food chemistry 2014, 148, 162-169.